Test Reduction for Power Density Emitted by Handset mmWave Antenna Arrays

Zhekov, Stanislav Stefanov; Zhao, Kun; Franek, Ondrej; Zhang, Shuai

Published in:
IEEE Access

DOI (link to publication from Publisher):
10.1109/ACCESS.2021.3055420

Publication date:
2021

Test Reduction for Power Density Emitted by Handset mmWave Antenna Arrays

Stanislav Stefanov Zhekov, Kun Zhao, Ondrej Franek, and Shuai Zhang

***Abstract*—The exposure to electromagnetic field (EMF) from phased antenna arrays integrated into wireless devices operating at the millimeter-wave (mmWave) part of the spectrum should be evaluated in terms of power density (PD). Two aspects related to test reduction when evaluating the radiation from handset antenna arrays are considered. First, the peak PD decay with the distance from 4-elements antenna arrays is analyzed. The focus is on finding the size of the volume around the handset beyond which the PD is so low that its measurement can be omitted. By limiting the measurements to the inside of the exposed volume, the total test time is reduced. Antenna configurations that are representative for current trends in handset technology are chosen: arrays of half-wavelength dipoles and patches operating at 26 GHz, 28 GHz, and 39 GHz, and having inter-element spacing either 0.5λ or 0.9λ. The second investigation aims to determine the critical distance between two 4-elements phased arrays for which the peak PD when the two arrays operate simultaneously is similar to the peak PD when only one array operates at the time. The study shows the configurations for which the number of tests can be reduced while having sufficiently accurate results.**

***Index Terms*—Antenna array, decoupling, dipole, exposed volume, handset, mmWave, patch, power density, test reduction.**

I. Introduction

The fifth-generation (5G) mobile communication systems targets to satisfy, among others, multi gigabit-per-second data rates, lower latency, and lower energy consumption [1]–[3]. The need for wide frequency bandwidths for achieving the high data rate of 5G cellular systems has pushed towards the employment of the mmWave part of the electromagnetic spectrum (above 24 GHz [4]), where large amount of raw bandwidth is available [1]. The small wavelengths in this part of the spectrum enable miniaturizing the size of the antennas and integration of phased antenna arrays into the user equipment (UE) [1], [5]. However, due to the limited space for deployment of antennas in mobile devices and need of having radio frequency (RF) chains for all mobile technologies (due to their coexistence) in them, likely a mmWave UE will have a few antenna panels and each panel will be composed of multiple antenna elements (four elements are currently considered [6]).

The maximum transmit power by mobile device, affecting the capacity of the system and the radio coverage [7], [8], is limited by the relevant RF EMF exposure safety regulations [9], [10]. That is, the devices need to be tested in order to ensure limited human exposure to EMF. Exposure limits, for the protection of humans from excessive temperature elevation at the body surface, have been defined by the: 1) International Commission on Non-Ionizing Radiation (ICNIRP) [11]; 2) Federal Communications Commission (FCC) [12] (proposed changes in [13], [14]); and 3) IEEE [15]. At low frequencies the restrictions on the EMF exposure for UE are specified through the metric specific absorption rate (SAR) in W/kg. At high frequencies, the penetration depth of EMF into the human body is smaller and therefore absorption in the human tissue is more superficial and the PD metric is used for restricting the exposure [9], [10], [16]–[18] More specifically, the epithelial (IEEE) or the transmitted (ICNIRP) PD is used as new basic restriction/dosimetric reference limit for local exposure instead of SAR at frequencies above 6 GHz [17], [18]. Incident PD (IPD) is used as a exposure reference level, where the spatial averaging area of IPD over 6 GHz is needed to correlate with resultant skin temperature elevation [16], [17]. Due to practical difficulties in assessing the transmitted PD in the superficial tissue (evaluation of transmitted PD by means of measurements in a very thin layer of skin is not feasible), limits on reference levels in terms of incident PD in free space can be used [18].

A literature review regarding the existing knowledge of the effects of non-ionizing mmWave radiation on the human body can be found in [19]. The implication of the move from SAR to PD at higher frequencies has been investigated in [7]. Various studies at mmWave frequncies can be found in the literature: 1) EMF exposure of patch antenna arrays has been discussed in [9]; 2) maximum equivalent isotropically radiated power (EIRP) in [5], [10]; and 3) the relationship between incident power density and skin temperature elevation have been presented in [16], [17], [20]. However, the exposed volume around antenna array has not been thoroughly discussed in any of theses studies.

Regarding PD testing at high frequency, in the open literature one can find: 1) description of the state-of-the-art measurement techniques and test approaches for evaluating the incident PD have been given in [21]; 2) scalar- and vector-based measurement systems for RF EMF compliance assessment have been discussed in [22], while techniques for evaluation of the PD in the vicinity of the antenna in [23]–[25]; 3) accuracy of a method for assessing the PD in a close proximity to a wireless device has been discussed in [26]; and 4) investigation on the the distance from the RF source at which meaningful free space PD assessments can be performed has been shown in [18]. Also, in [18] has been shown that at frequencies around 30 GHz, free space PD assessments should be enough to ensure safety limits

The authors are with the Department of Electronic Systems, Technical Faculty of IT and Design, Aalborg University, Aalborg, Denmark (e-mail: stz@es.aau.dk; kz@es.aau.dk; of@es.aau.dk; sz@es.aau.dk)

Kun Zhao is also with the R&D Center Europe Lund Laboratory, Sony Corporation, SE-221 88 Lund, Sweden (e-mail: kun.1.zhao@sony.com)

compliance. Free space PD is also considered in this paper, however, our focus is on its decay with the distance (over several wavelengths) from the antenna array.

Mobile terminals need to be tested in order to ensure that people health is not in risk. Taking into account that the measurements of PD are time-consuming [22], [26] together with necessity to measure large amount of phones means that the excessive amount of time will be spend for testing. Shortening the test time can be achieved simply by limiting the test volume, i.e. reducing the number of measurements. Due to that, systematic studying the size of the volume, out of which the local EMF exposure of antenna array is below certain threshold, is performed in this paper.

Another study conducted in this paper is on determining the critical distance between two antenna arrays, integrated into UE. The critical distance is the distance ensuring that the combined incident PD (when the two arrays operate simultaneously) is similar to the individual incident PD (when only one array operate at the time). To the authors' best knowledge no such study has previously been presented. The importance of the investigation follows from the fact that if it is known in advance that the distance between two arrays is large enough to be decoupled then the test of the PD when they operate simultaneously can be omitted. Thus, resources and test time can be saved.

The aim of the paper is that - providing information that can be used for speeding-up the test of PD radiated from phased antenna arrays intended to be deployed in UE operating at mmWave frequencies. Antenna arrays containing 4-elements (this is expected typical numbers of radiators at the studied frequency for handheld UE and portable devices [6], [18]) are employed in the study and several parameters (type of radiator, frequency, inter-element distance, beamforming precodes, and position of the antenna array along the edge of the ground plane) are varied for the sake of having a large number of study cases. All investigations were conducted by using CST Microwave Studio 2019.

The paper is organized as follows. Section II gives information about the evaluation of the PD. The methodology employed for investigating the size of the exposed volume is described in Section III while in Section IV are presented the results from the study. Details about the investigation focused on finding the critical distance between two antenna arrays are provided in Section V while results from the study are given in Section VI. Finally, conclusions are provided in Section VII.

II. Power Density Calculation

The PD $\vec{S}$ throughout this paper is defined as time-average Poynting vector. The equation for calculating the PD is:

$$\vec{S} = \frac{1}{2}\mathrm{Re}[\vec{E} \times \vec{H}^*] \quad (1)$$

where $\vec{E}$ and $\vec{H}$ are the complex electric and magnetic field, respectively; (*) indicates complex conjugate. In order to remove the direction dependent sign of $\vec{S}$, the absolute value of each component ($|S_x|$, $|S_y|$, and $|S_z|$) of the vector is used in the rest of the paper. Each of the three components of the power density $|S_x|$, $|S_y|$, and $|S_z|$ as well as the norm $||S||$ were considered in the studies.

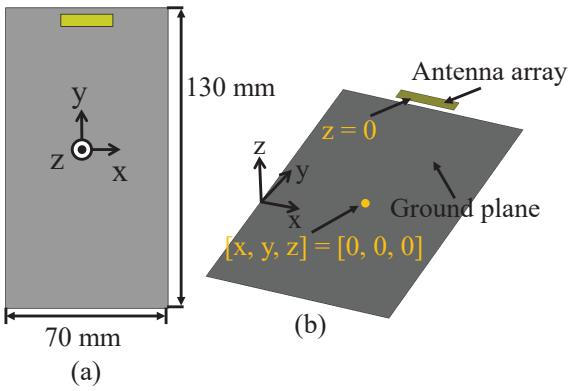

Fig. 1: Example for an on-ground antenna array (presented as one monolithic structure with yellow color) located symmetrically with respect to the ground plane along $x-$axis: (a) front view, and (b) perspective view.

The antenna elements building the arrays were designed in such a way that they have return loss better than 10 dB at the frequency of interest, when feeding them with signals with the same amplitude and phase of 0°. All presented PD results are normalized to 23 dBm (0.2 W) of radiated power from the antenna arrays; 23 dBm was taken because this is the maximum allowed transmitted power for 5G UE [4]. The normalization was conducted just by multiplying $|S|$ with 23 dBm and diving the results to the simulated radiated power for each studied beamforming separately. Through the normalization the effect of return loss, mutual coupling and ohmic losses for each array on the PD is removed. Thus, it was possible to compare the PD from different arrays. It should be mentioned that the exact number used for normalization is not important for the study, since we are interested in the relative value as discussed in the next section.

III. Methodology for the Exposed Volume Study

This study aims to analyze the power density distribution of different array configurations in order to delimit the volume out of which the PD is beneath -13 dB with respect to the maximum. In this way, the measurements can be avoided outside this box (exposed volume).

A. Phased antenna arrays

Linear phased antenna arrays consisting of 4-radiating elements were used in the study. The arrays can be separated into two categories: 1) on-ground array - an array having ground plane under the antenna elements (Fig. 1 and Fig. 2(a), (b)); and 2) off-ground array - an array having no ground plane under the antenna elements (Fig. 2(c)). On-ground arrays were built from half-wavelength dipoles or square patches (Fig. 2(a), (b)), while the off-ground phased arrays contained half-wavelength dipoles (Fig. 2(c) - the array and the ground plane lie on the same XY plane). The labels for the antenna arrays used in the rest of the paper are given in Fig. 2. Two different types of antennas were employed in order to investigate the

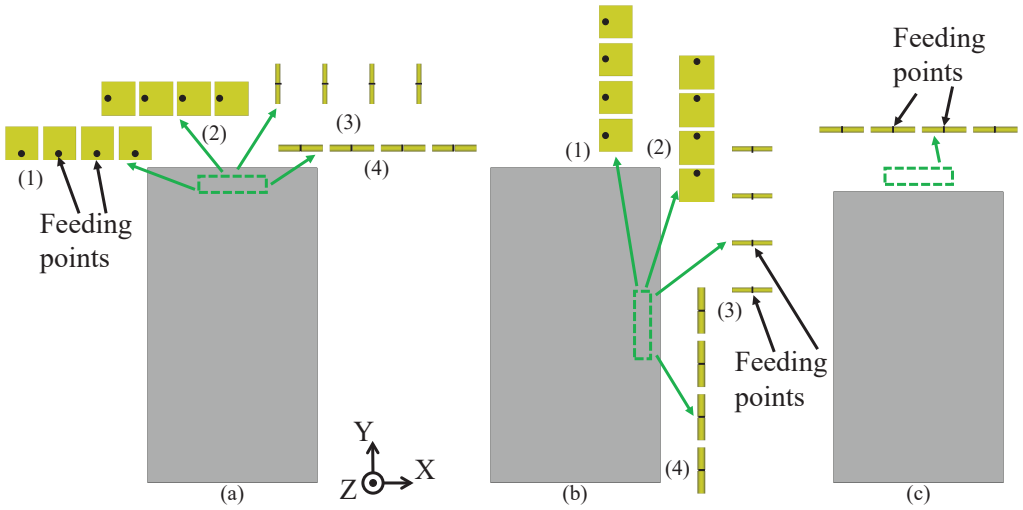

Fig. 2: Studied on-ground arrays are given in (a), (b), while off-ground in (c). The antenna array contains four patches in (a)(1) and (2), and (b)(1) and (2), and four dipoles in (a)(3) and (4), and (b)(3) and (4), and (c). The following notation is used thought the paper: in (a) are given on-ground arrays along the short edge of the ground plane ($x-$axis), as (1) is named Patch1, (2) Patch2, (3) Dipole1, and (4) Dipole2; in (b) are given on-ground arrays along the long edge of the ground plane ($y-$axis), as (1) is named Patch3, (2) Patch4, (3) Dipole3, and (4) Dipole4; and in (c) is given off-ground array (along $x-$axis), named Dipole5 - for off-ground arrays (the array and the ground plane lie on the same XY plane) only placements along the short edge of the ground plane are considered. In this figure only the placements (Position1) in the center of the short and long edge of the ground plane are presented.

change in the size of the exposed volume with the change of the radiator. Also two inter-element distances - 0.5λ and 0.9λ (λ is the free space wavelength) were considered in the study.

Patch and dipole antennas were selected because they are simple and well known antennas. More importantly, they are expected to be used for building 5G arrays for mobile terminals and portable wireless devices [18]. Both antennas and ground plane were made of copper. In all simulation models air was used for substrate (no dielectric loss). This is considered the worst case scenario for the exposure area since there is no confining of the transmitted power density from the antenna array in the substrate.

For the on-ground dipoles and patches both linear polarizations were considered in the study (Fig. 2(a), (b)). For the off-ground dipoles only one polarization was investigated (Fig. 2(c)); for the other polarization, larger part of the ground plane would need to be cut out in order to fit the dipoles and since the ground plane is a limited resource in mobile terminals this case is considered unlikely to occur.

B. Mock-up

As shown in Fig. 1, no matter on- or off-ground array is considered, the width of the entire structure is of 70 mm and the length is of 130 mm (see also Fig. 2). For dipole arrays - the distance between the dipole and the ground plane, in $z-$direction, was of $\lambda/4$ to maximize the field radiated from the antenna (not shown). For off-ground array also distance of $\lambda/4$ was used between the dipoles and the ground plane (in $y-$direction; in this case the dipole are beyond the ground plane), as shown in Fig. 3(c). For the off-ground array the length of the ground plane is trimmed individually at each frequency in order to keep the length of the entire structure (ground plane and antenna array) of 130 mm.

Two different positions of the on-ground antenna arrays along both short (the antenna arrays in Fig. 2(a)) and long edge (the antenna arrays from Fig. 2(b)) of the ground plane and two different placements of the off-ground arrays along the short edge (the antenna arrays from Fig. 2(c)) were considered in the study. Scheme of the positions of the antenna array along the edge of the ground plane is shown in Fig. 3. The positions of the array are as follows:

- Position1 - on-ground array is in the center of short/long edge along $x-$/$y-$axis regardless whether the inter-element distance is of 0.5λ or of 0.9λ (Fig. 3(a), (b), left-hand side in each subfigure). For off-ground array the same position is studied but only along the short edge (Fig. 3(c), left-hand side).
- Position2: 1) on-/off-ground array along the short edge of the ground plane - the distance from the right edge of the right most antenna in the array, when the inter-element distance is of 0.9λ, to the long edge of the ground plane is of $\lambda/4$ (Fig. 3(a), (c), right-hand side in each subfigure); 2) on-ground array along the long edge of the ground plane - the distance from the top edge of the top most antenna in the array, when the inter-element distance is of 0.9λ, to the short edge of the ground plane is of $\lambda/4$ (Fig. 3(b), right-hand side). For this position, in all cases, for 0.5λ inter-element distance the array has the same center as for 0.9λ.

As shown in Fig. 3: 1) for on-ground array along the short edge of the ground plane - the distance ($y-$direction) between the edge of the ground plane and the edge of the antenna elements is of $\lambda/4$; for on-ground array along the long edge of the ground plane - the distance ($x-$direction) between the right edge of the ground plane and the right edge of the antenna elements is of $\lambda/4$; and 2) for off-ground array - the distance

($y-$direction) between the edge of the ground plane and the edge of the antenna elements is of $\lambda/4$ (the array and the ground plane lie on the same XY plane). Thus, the electrical distance between the edge of antenna elements and the edge of ground plane was kept the same for all frequencies of interest and the same among all antenna arrays.

C. Parameters in the investigation

So far it has been mentioned that antenna elements, inter-element distance and position of the array along the edge of the ground plane were parameters varied for the sake of the study. There are two more parameters involved in the investigation as follows:

1) frequency: 26 GHz, 28 GHz, and 39 GHz.

2) beam-forming precoding - the emitted power density was evaluated for multiple different excitations of the array. The amplitude of the signal feeding each antenna element was kept 1 (i.e. the same) but the phase was progressively changed from one antenna element to the next one. That is, feeding the antenna elements with $w_i = [1, 1e^{-j\phi}, 1e^{-2j\phi}, 1e^{-3j\phi}]$ where the phase shift ϕ takes value of 0°, ±30°, ±60°, ±90°, ±120°, ±150°. All these excitations were used in order to find the worst case scenario.

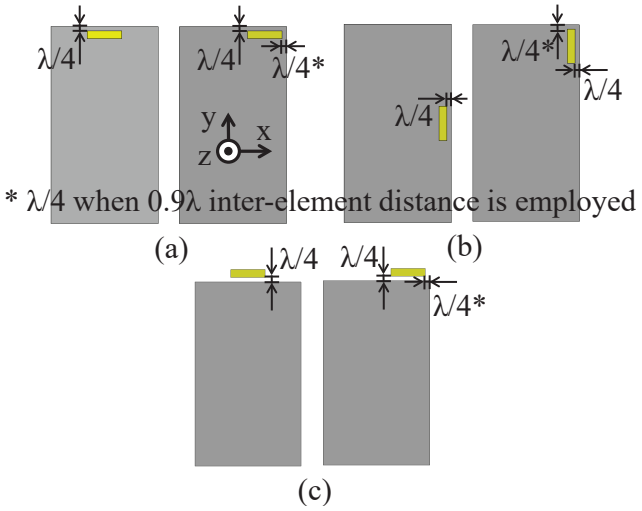

Fig. 3: Studied positions of the antenna arrays (presented as one monolithic structure with yellow color): (a) on-ground array along the short edge of the ground plane and (b) along the long edge; (c) off-ground array along the short edge. On the left-hand side in each subfigure is presented Position1, while on the right-hand side - Position2. For on-ground cases, the array is above the ground plane in $z-$direction, while for off-ground case the array and ground plane lie in the same XY plane.

D. Exposed volume

The origin of the coordinate system, used for presenting the results in the paper, is given in Fig. 1. The x and y coordinates of the origin match with the center of the structure in XY plane; $z = 0$ match with the position of the top surface of the antenna elements (regardless whether it is dipole or patch) along z-axis (see Fig. 1 where $z = 0$ is also marked on the top surface of the array).

In order to determine the size of the exposed volume (parallelepiped encompassing the antenna array), it is needed to find the x, y, z-coordinate at which $|S_x|, |S_y|, |S_z|$ values along $x-, y-, z$-axis (and $||S||$ along all axis), respectively, are 13 dB below the (5% of) global peak $|S_x|, |S_y|, |S_z|$ and $||S||$ values regardless of the beam-forming precoding. The selection for using -13 dB for finding the boundary is due to the fact that this is considered sufficiently low level, i.e. out of the exposed volume there is no need to conduct PD tests. This number is related to the test exclusion criteria for SAR from multiple-sources. If one source contributes less than 5% (-13 dB) to the radiation of other source, then the measurement can only be applied to the second source while the first source (having less than 5%) contribution is neglected [27].

The global peak value for each component and for the norm of the PD was sought on the planes located 1 mm away from the tight bounding box enclosing the structure. During the test, the field probe should not be in contact with the antenna array and therefore certain minimum distance should be kept. However, if the minimum distance is large then the global peak PD will be low. This together with the fact that away from the antenna the field decays slower, than close to it, will lead to a very large exposed volume (in the way it is defined). That is, we wanted to include the fast decay of the field without starting the sampling too close to the antenna array. Due to that, we considered that distance of 1 mm is acceptable.

The planes along with their coordinates are shown in Fig. 4 (only one on-ground case is presented). They are 1 mm away: 1) from the ground plane in $x-$direction - YZ plane; 2) from the ground plane in $y-$direction for on- and from the antenna array for off-ground cases (in order to be able to use the same XZ plane, as for on-ground array, the length of the structure in the off-ground case is kept 130 mm by trimming the ground plane) - XZ plane; and 3) from the antenna array in $z-$direction ($z = 0$ match with the antenna top surface) - XY plane. The global peak value for each $|S_x|$, $|S_y|$, $|S_z|$, and $||S||$ is the highest value found on these three planes. Then the global peak values were used for finding the boundary for the corresponding component (normal component) of the power density along the corresponding coordinate axis; for the norm, the same global peak value was used for finding the boundary along each coordinate axis.

IV. Results for the Exposed Volume

A. On-ground antenna arrays

The peak value of each component $|S_x|$, $|S_y|$, and $|S_z|$ found on the planes normal to the corresponding component of the PD/coordinate axis for Patch1 and Dipole1 with 0.5λ inter-element distance, operating at 28 GHz, placed in Position1, for each studied beam-forming precoding is shown in Fig. 5. Also, the peak value of the norm $||S||$ found on each plane is presented. The coordinates of the edges of the structure in each direction are given with purple solid lines. The gray solid line passes at the value corresponding to 13-dB below the global peak value for each of the components and norm of the PD. The PD at points located within a box with coordinates: 1)

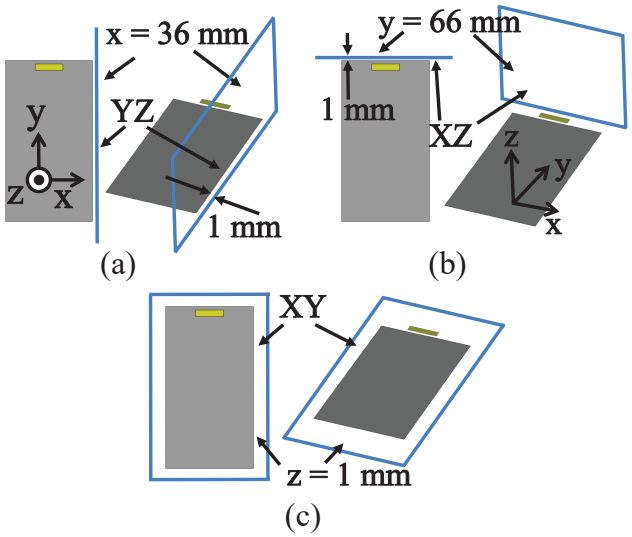

Fig. 4: Planes on which the global peak PD is sought: (a) YZ plane, (b) XZ plane, and (c) XY plane. The example is for on-ground array (presented as one monolithic structure with yellow color) placed in the middle of the short edge of the ground plane, but the same planes are used in all other scenarios, i.e. no matter the type of the array and its position. The origin of the coordinate system is given in Fig. 1.

x from -35 mm to 35 mm; 2) y from -65 mm to 65 mm; and 3) z from -3 mm to 0 mm was not taken into account. In this way PD around the ground plane and between the array and the ground plane is excluded. It is assumed that tests can be conducted 1 mm away from this box. This means that the data between the purple solid lines (and in general in the entire study) do not take into account the PD within the above mentioned box.

From Fig. 5, one can see how the peak value of the PD decays with the distance from the antenna array and how this decay depends on the used beam-forming precoding. For the two presented examples: 1) for Patch1 array the value in the peak position varies - for $|S_x|$ between 596 W/m^2 (obtained for 0° phase difference between the array elements) and 2855 W/m^2 (for ±120°), for $|S_y|$ between 1250 W/m^2 (for 0°) and 3403 W/m^2 (for ±150°), for $|S_z|$ between 2023 W/m^2 (for 0°) and 3400 W/m^2 (for ±150°), and for $||S||$ between 2184 W/m^2 (for 0°) and 4435 W/m^2 (for ±150°); and 2) for Dipole1 array - for $|S_x|$ between 1275 W/m^2 (for 0°) and 2709 W/m^2 (for ±150°), for $|S_y|$ between 755 W/m^2 (for ±120°) and 1098 W/m^2 (for ±30°), for $|S_z|$ between 3649 W/m^2 (for ±150°) and 3785 W/m^2 (for ±60°), and for $||S||$ between 3725 W/m^2 (for 0°) and 4092 W/m^2 (for ±150°). Difference in the positions of the boundaries between the two presented antenna arrays can be seen. $|S_z|$ and $||S||$ in -z-direction are very weak, i.e. the back radiation is insignificant since the ground plane under the array acts as a shield. This is the case, as one can expect, for all on-ground arrays.

Table I shows the worst case scenario for the coordinates of the boundary found for each component of $|S|$ as well as for the norm $||S||$ of the PD among all on-ground antenna arrays and among all beam-forming precodings.

1) $|S_x|$ and $||S||$ along x-axis: For antenna array along the short edge of the ground plane, due to its moving (along x-axis) one can see in Table I significant difference in the coordinate of the boundary for Position1 and Position2. For antenna array along the long edge of the ground plane the move (it is along y-axis) between the two positions has almost no impact on the coordinate of this boundary. As expected the width (i.e. distance between the boundaries along x-axis) of the exposed volume decreases with increasing the operation frequency. One can see that the width decreases with decreasing the inter-element distance. It is observed that the exposed volume has a smaller width when the norm of PD is considered than when $|S_x|$ (the normal component in this case).

2) $|S_y|$ and $||S||$ along y-axis: As one can see in Table I the length (i.e. distance between the boundaries along y-axis) of the exposed volume for antenna array along the short edge of the ground plane is similar to the width (when comparing the corresponding positions) for antenna array along the long edge and vice versa. The length of the exposed volume decreases with increasing the operation frequency and with decreasing the inter-element distance. The exposed volume has a smaller length when the norm of PD is considered than when $|S_y|$ (the normal component in this case).

3) $|S_z|$ and $||S||$ along z-axis: Table I shows data only for the coordinate of the boundary in positive z-direction since the PD behind the ground plane is much lower than 5% of the global peak value of the PD. The height of the exposed volume decrease with increasing the frequency. Also it decreases with decreasing the inter-element spacing. Regardless whether the array is along short or long edge of the ground plane and whether is at Position1 or at Position2 the coordinate of the boundary is not affected. The exposed volume has smaller height when $||S||$ is considered than when $|S_z|$.

4) Size of the exposed volume: The coordinates from Table I define the exposed volume with parallelepiped shape and size given in Table II. Out of the parallelepiped (its position is defined through the position of the array and the coordinates of the boundaries): 1) with dimensions shown in the top part in Table II, each component $|S_x|$, $|S_y|$, and $|S_z|$ is at least 13-dB lower than the corresponding global peak values regardless of the studied beam-forming precoding; and 2) with dimensions shown in the bottom part in Table II, $||S||$ is at least 13-dB lower than the corresponding global peak values regardless of the studied beam-forming precoding. Out of these volumes no tests are needed because the PD has a low enough value. It should be kept in mind that the global peak value and the position of the boundary (in the paper the worst case scenario is presented) depends on the phase shift assigned to the antenna elements. However, general discussion on which progressive phase shift (beam-forming precoding) leads to the global peak value and which progressive phase shift defines the coordinate of the boundaries of the exposed volume is omitted for the sake of brevity.

5) Symmetry and position dependence of the boundaries: In order to further investigate the possibility for test reduction, we checked whether: 1) the distances between the array boundaries and exposed volume boundaries along certain

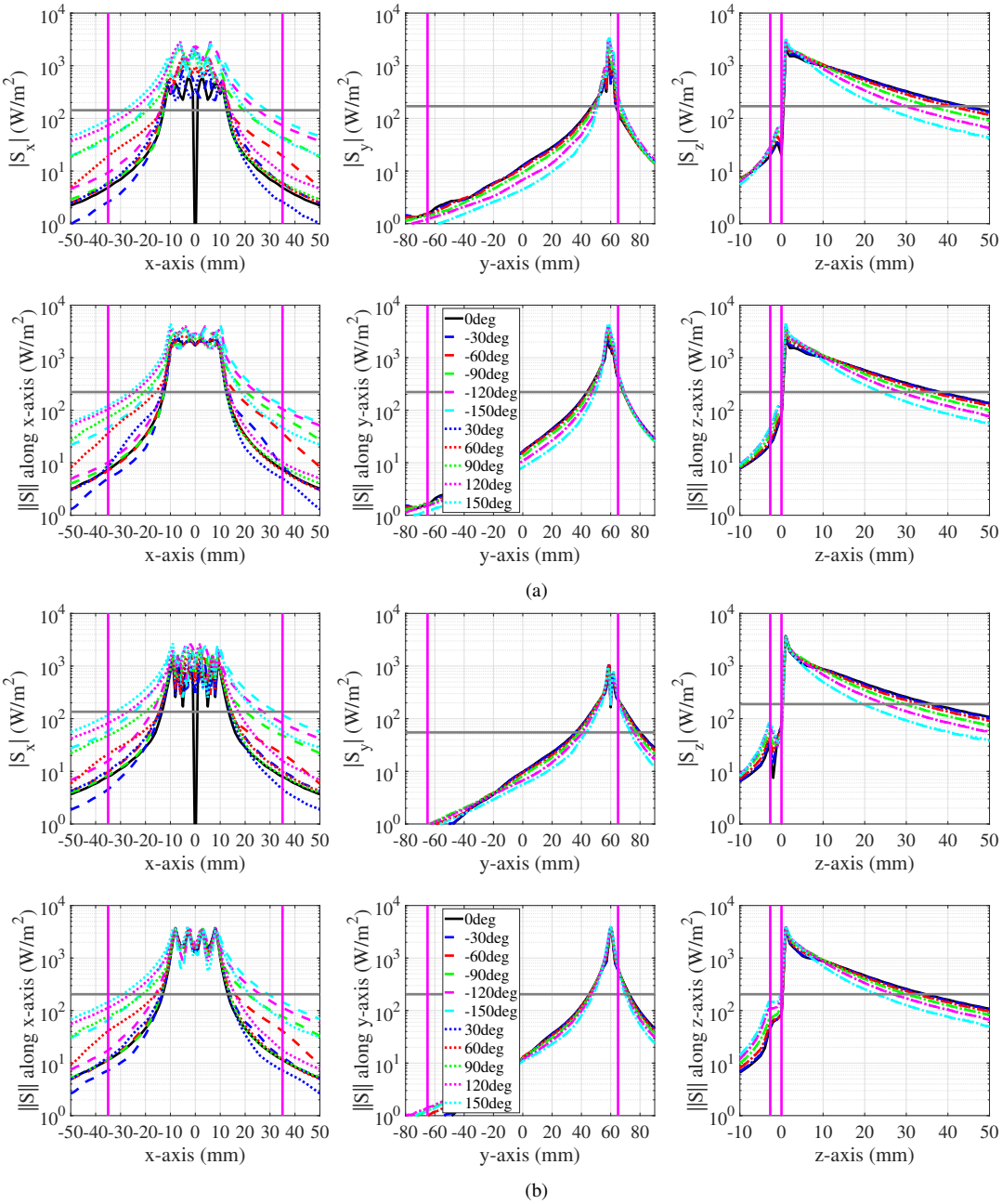

Fig. 5: Decay of the maximum value of each components of $|S|$ (top graphs) and norm $||S||$ (bottom graphs) with the distance for antenna array with 0.5λ inter-element distance, operating at 28 GHz, placed in Position1, for each studied beam-forming precoding: (a) Patch1, and (b) Dipole1.

axis are equal - symmetry of the boundaries (there is no symmetry along z-axis for on-ground arrays); and 2) whether the width/length (and height for the off-ground array) of the exposed volume varies with the position of the antenna array along the ground plane - position dependence of the boundaries. The following criteria were applied: 1) symmetry: 1.1) whether the difference between the distance from the left edge of the array to the left boundary of the exposed volume and the distance from the right edge of the array to the right boundary of the exposed volume is less than or equal to 3 mm - symmetry along x-axis; 1.2) whether the difference between the distance from the top edge of the array to the top boundary of the exposed volume and the distance from the bottom edge of the array to the bottom boundary of the exposed volume is less than or equal to 3 mm - symmetry along y-axis; and 2) position dependence: whether the difference in the width/length (and height for the off-ground array) of the exposed volume between Position1 and Position2 is less than or equal to 3 mm - for this can be judged also from Table II.

The presence of symmetry in the results along a certain axis means that the power density only in half of the space needs to be measured (in the other half it is the same) which, in turn, will lead to 50% reduction in the number of needed tests. The position independence means that width/length (and

TABLE I: Coordinates of the boundary of the exposed volume found for each components and norm of the PD among all studied on-ground arrays and beam-forming precodings. For $|S_x|$, $|S_y|$ as well as $||S||$ along x-axis and y-axis two numbers are presented giving the coordinate of the boundary on each side of the array along the corresponding axis. For $|S_z|$ and $||S||$ along z-axis there is only one number showing the coordinate of the boundary in +z-direction (the back radiation, i.e. the one in -z-direction is negligible and the boundary in that direction can be consider located right behind the ground plane).

PD	Array Position	Array along short edge						Array along long edge					
		26 GHz		28 GHz		39 GHz		26 GHz		28 GHz		39 GHz	
		0.5λ	0.9λ	0.5λ	0.9λ	0.5λ	0.9λ	0.5λ	0.9λ	0.5λ	0.9λ	0.5λ	0.9λ
		Coordinates of the boundaries (mm)											
$\|S_x\|$ along x-axis	1	-35 35	-40 40	-33 33	-38 38	-26 26	-29 29	3 54	-7 63	5 54	-4 61	11 51	4 56
	2	-18 51	-26 54	-15 50	-22 53	-3 48	-8 50	3 54	-8 64	5 54	-5 62	11 51	4 57
$\|\|S\|\|$ along x-axis	1	-31 31	-31 31	-30 30	-29 29	-24 24	-25 25	13 46	5 44	14 46	6 45	19 44	9 45
	2	-15 48	-17 45	-12 48	-13 45	-1 46	-4 45	13 46	5 45	14 46	6 46	19 44	10 46
$\|S_y\|$ along y-axis	1	33 84	23 93	35 84	26 92	41 81	34 86	-35 35	-40 40	-33 33	-38 38	-26 26	-29 29
	2	33 84	22 94	35 84	25 93	41 81	34 87	12 81	4 84	15 81	8 83	27 78	22 80
$\|\|S\|\|$ along y-axis	1	43 76	35 74	43 76	36 75	49 74	39 75	-31 31	-31 31	-30 30	-29 29	-24 24	-24 24
	2	43 76	35 75	44 76	36 76	49 74	40 76	15 78	13 75	18 78	17 75	29 76	26 75
$\|S_z\|$ along z-axis	1	47	72	45	71	42	69	46	73	44	70	41	70
	2	46	73	45	71	42	70	46	73	44	71	42	70
$\|\|S\|\|$ along z-axis	1	41	67	38	65	32	59	40	67	38	64	32	59
	2	40	68	38	65	32	60	40	67	38	64	32	60

TABLE II: Size of the exposed volume for the components (top part) and for norm (bottom) of the PD.

Position	Array along short edge						Array along long edge					
	26 GHz		28 GHz		39 GHz		26 GHz		28 GHz		39 GHz	
	0.5λ	0.9λ	0.5λ	0.9λ	0.5λ	0.9λ	0.5λ	0.9λ	0.5λ	0.9λ	0.5λ	0.9λ
	Size (X x Y x Z) of the exposed volume for the components of $\|S\|$ (mm^3)											
1	70 x 51 x 47	80 x 70 x 72	66 x 49 x 45	76 x 66 x 71	52 x 40 x 42	58 x 52 x 69	51 x 70 x 46	70 x 80 x 73	49 x 66 x 44	65 x 76 x 70	40 x 52 x 41	52 x 58 x 70
2	69 x 51 x 46	80 x 72 x 73	65 x 49 x 45	75 x 68 x 71	51 x 40 x 42	58 x 53 x 70	51 x 69 x 46	72 x 80 x 73	49 x 66 x 44	67 x 75 x 71	40 x 51 x 42	53 x 58 x 70
	Size (X x Y x Z) of the exposed volume for the norm $\|\|S\|\|$ (mm^3)											
1	62 x 33 x 41	62 x 39 x 67	60 x 33 x 38	58 x 39 x 65	48 x 25 x 32	50 x 36 x 59	33 x 62 x 40	39 x 62 x 67	32 x 60 x 38	39 x 58 x 64	25 x 48 x 32	36 x 48 x 59
2	63 x 33 x 40	62 x 40 x 68	60 x 32 x 38	58 x 40 x 65	47 x 25 x 32	49 x 36 x 60	33 x 63 x 40	40 x 62 x 67	32 x 60 x 38	40 x 58 x 64	25 x 47 x 32	36 x 49 x 60

height for the off-ground array) of the exposed volume is similar regardless of the location of the antenna array along the ground plane.

In most of the studied cases, for $|S_x|$ and $||S||$ along x-axis symmetry of the boundaries with respect to the antenna array, positioned along the short edge of the ground plane, is observed. This is expectable for Position1 (Patch1, Dipole1, and Dipole2 are symmetrical in terms of structure and feeding - the names of the antenna arrays are given in Fig. 2) but the finding that the boundaries are symmetrically positioned is important for Position2 where the antenna array is asymmetrical with respect to the edge of the ground plane along $x-$axis. Exceptions are found for Patch2 for both $|S_x|$ and $||S||$ in x-direction for 0.9λ inter-element distance. Some position dependence (i.e. greater than 3 mm) for the width of the exposed volume is observed for Patch2 and for Dipole2 for $|S_x|$ for 0.9λ inter-element distance.

There is no symmetry between the two boundaries along y-axis for $|S_y|$ and $||S||$ for Patch1 (in y-direction the feeding is not symmetrical placed with respect to the side of the antenna), while Patch2 exhibits symmetry. For Dipole1 no symmetry for $|S_y|$ (and for $||S||$ in one case) is observed while for Dipole2 symmetrical results are seen (except for $|S_y|$ in some cases). Position independence of the length of the exposed volume in all cases is observed (some exception is seen for Dipole1). The discussion for symmetry and position dependence of the boundaries for antenna arrays along the long edge of the ground plane is inverted to that for the arrays along the short edge of the ground plane. It should just be kept in mind that the analysis for Patch3/Patch4/Dipole3/Dipole4 for long edge placements correspond to that for Patch1/Patch2/Dipole1/Dipole2 for short edge placements.

B. Off-ground antenna arrays

Example of the decay with distance of the peak value of each component of the PD and the norm along the corresponding axes for Dipole5 at 28 GHz for Position1 for 0.5λ inter-element spacing, for each studied beam-forming precoding is shown in Fig. 6. Regarding the figure, all descriptions are the same as the ones explained when discussing Fig. 5. The only difference is that a plane, within which the power density is excluded, is used (the same x- and y-coordinates as for the box for the on-ground array and the z-coordinate is 0 mm) instead of a box.

For the presented example the value in the peak position varies - for $|S_x|$ between 922 W/m^2 (obtained for 0° phase difference between the array elements) and 2299 W/m^2 (for $\pm 120^\circ$), for $|S_y|$ between 3023 W/m^2 (for 0°) and 4423 W/m^2 (for $\pm 150^\circ$), for $|S_z|$ between 2890 W/m^2 (for 0°) and 3974

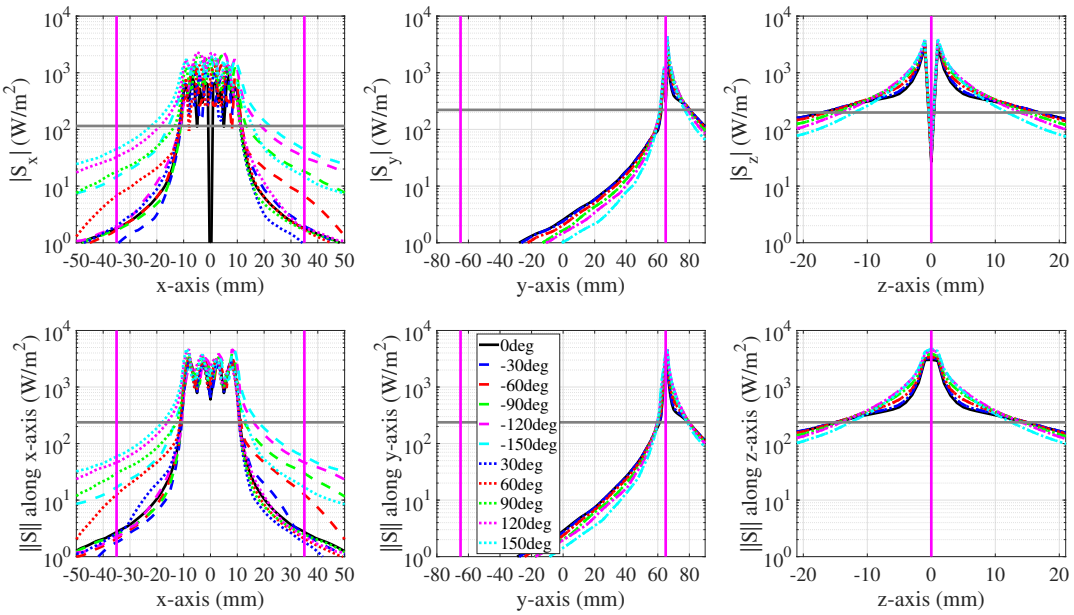

Fig. 6: Decay of the maximum value of each components of $|S|$ (top graphs) and of $||S||$ (bottom graphs) with the distance for Dipole5 array with 0.5λ inter-element distance, operating at 28 GHz, placed in Position1, for each studied beam-forming precoding.

W/m^2 (for $\pm 150°$), and for $||S||$ between 3041 W/m^2 (for $0°$) and 4751 W/m^2 (for $\pm 150°$). Due to the fact that there is no ground plane under the antenna array, the radiation in -z-direction (back radiation) is the same as the radiation in z-direction.

1) Boundaries of the exposed volume: Table III shows the positions of the boundary for each component of $|S|$ as well as for $||S||$. The difference between the results for the 0.5λ and 0.9λ inter-element distance is some millimeters. The position of the antenna array has negligible impact on the position of the boundary in y-direction. Due to almost perfect symmetry of the antenna array along z-axis the results in $+z$- and $-z$-direction are similar. The coordinate of the 13-dB boundary along z-axis does not vary with the position of the antenna array.

The coordinates from Table III define two parallelepipeds with size: 1) 52 x 20 x 36 mm^3 out of it each component $|S_x|$, $|S_y|$, and $|S_z|$, and 2) 44 x 22 x 32 mm^3 out of it $||S||$ are at least 13-dB lower than the corresponding global peak values regardless of the beam-forming precoding, i.e. out of these volumes no tests are needed because the PD has a low enough value. The volume along $x-$ and $z-$axes is larger when the components of the PD are considered rather than the norm, while along $y-$axes the size of the two volumes is similar. As for the on-ground arrays, general discussion on which progressive phase shift (beam-forming precoding) leads to the global peak value and which progressive phase shift defines the coordinate of the boundaries of the exposed volume is omitted for the sake of brevity.

2) Symmetry and position dependence of the boundaries: For Dipole5 symmetrical boundaries, with respect to the antenna array, along x- and z-axis are observed, while the boundaries are non-symmetrical for $|S_y|$ and $||S||$ in y-direction. This means that the measurements along x- and z-axis can be halved, i.e. the tests can be reduced by 4-times. In all cases, position independence of the length, width, and height of the exposed volume is observed.

TABLE III: Coordinates of the boundary of the exposed volume found for each components and norm of the PD for Dipole5 array and among all studied beam-forming precodings. The two numbers in the cells give the coordinate of the boundary on each side of the array in the corresponding direction.

PD	Array Position	26 GHz		28 GHz		39 GHz	
		0.5λ	0.9λ	0.5λ	0.9λ	0.5λ	0.9λ
		Coordinates of the boundaries (mm)					
$\|S_x\|$ along x-axis	1	-23 23	-26 26	-23 23	-25 25	-18 18	-21 21
	2	-9 38	-11 39	-7 38	-8 40	3 39	1 41
$\|\|S\|\|$ along x-axis	1	-19 19	-21 21	-18 18	-20 20	-16 16	-16 16
	2	-5 33	-7 35	-3 34	-4 35	5 37	5 37
$\|S_y\|$ along y-axis	1	61 81	61 78	61 81	61 78	61 80	62 79
	2	61 81	61 78	61 81	61 78	61 80	62 79
$\|\|S\|\|$ along y-axis	1	59 81	60 78	59 80	60 78	60 80	60 79
	2	59 81	60 78	59 81	60 78	60 80	60 79
$\|S_z\|$ along z-axis	1	-17 18	-13 13	-18 17	-13 13	-17 17	-15 15
	2	-18 18	-13 13	-18 18	-13 13	-17 17	-15 15
$\|\|S\|\|$ along z-axis	1	-16 16	-13 12	-15 16	-13 13	-15 15	-14 14
	2	-16 16	-13 13	-16 16	-13 13	-15 15	-14 14

V. Methodology for the Array Decoupling Study

A frequency range 2 (FR2; this notation is used for referring to the frequency range 24250 MHz – 52600 MHz) UE likely

will be equipped with multiple antenna arrays located in the different locations within the phones in order to provide a good spherical coverage and avoid sever blockage loss from the user's hands. However, testing multiple antenna arrays when they are transmitting simultaneously will increase the test time. The goal of this study is to find the distance between different array configurations at which the two arrays are decoupled, so that it is sufficient to consider the maximum PD when only one array operates at the time.

A. Parameters in the study

Two phased antenna arrays with 4-elements each (the same on-ground dipoles and patches discussed before) were used in this study. The inter-element distance between the antenna elements for each arrays is of 0.5λ. The antenna arrays used in the study, along with their labels, are shown in Fig. 7. Two different orientations of the antenna arrays with respect to each other were considered: 1) parallel arrays - the two antenna arrays were placed along the short edge of the ground plane (Fig. 7 on the left-hand side of each subfigure) as $\lambda/4$ distance ($x-$direction) between the short edge of the ground plane and the top edge of the antenna elements is kept; and 2) perpendicular arrays - one array was placed along the short edge and the other array was placed along the long edge of the ground plane (Fig. 7 on the right-hand side of each subfigure) - for Array 1, $\lambda/4$ distance ($x-$direction) between the short edge of the ground plane and the top edge of the antenna elements is kept, while for Array 2, $\lambda/4$ distance ($y-$direction) is kept between the right edge of the antennas and the long edge of the ground plane. With d in Fig. 7 is labeled the distance between the two antenna arrays. In the parallel case, the two antennas were moved away from each other simultaneously, while in the perpendicular case Array 1 was kept at the same position (this position matches with Position2 for 0.5λ inter-element distance discussed in Section III) while Array2 was moved.

As one can see in Fig. 7, arrays built from the same type of on-ground antennas (i.e. dipole - dipole and patch - patch) with the same orientation/position of the feeding point with respect to the closest edge of the ground plane are considered.

Other parameters varied in the study were:

1) frequency: 26 GHz, 28 GHz, and 39 GHz.

2) beam-forming precoding - for single array case (one array transmits at the time) the antenna elements are fed with signals with the same magnitude but with progressive phase shift between antenna elements of $0°$, $\pm30°$, $\pm60°$, $\pm90°$, $\pm120°$, $\pm150°$; for dual array case (both arrays transmit simultaneously) all combinations of signals with the same magnitude but progressive phase shifts $0°$, $\pm30°$, $\pm60°$, $\pm90°$, $\pm120°$, $\pm150°$ (having the same sign for Array1 and Array2 or opposite) were used for feeding the antenna elements of the two arrays. All these excitations were used in order to find the worst case scenario.

B. Criterion for considering the arrays decoupled

The same as discussed before, the maximum value of $|S_x|$, $|S_y|$, $|S_z|$, and $||S||$ was simultaneously sought on the three planes shown in Fig. 4 and from the three found values only the highest one (for each component and the norm for each array) was used in the study. The distance d between the two antenna arrays was increased with step of 0.5λ until the maximum value for $|S_x|$, $|S_y|$, $|S_z|$, and $||S||$ obtained when the two arrays are operating simultaneously differs less than 5% from the maximum value for $|S_x|$, $|S_y|$, $|S_z|$, and $||S||$ when the two arrays are operating separately, respectively. The minimum distance, for which the latter is achieved, is the critical distance and it is considered that the antenna arrays influence each other insignificantly, i.e. they are decoupled. The reason to select 5% (-13 dB) is the same as when discussing the exposed volume (test exclusion criteria for SAR from multiple-sources).

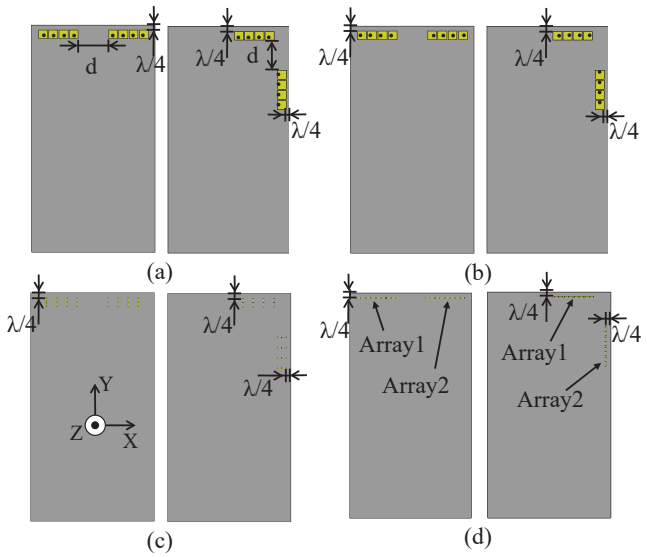

Fig. 7: Studied two on-ground arrays: (a) Patch1, (b) Patch2, (c) Dipole1, and (d) Dipole2. In each subfigure on the left-hand side is presented the parallel case and on the right-hand side the perpendicular case.

VI. Results for Array Decoupling

Example for decoupling of Dipole2 arrays in parallel case at 28 GHz is presented in Fig. 8, as the purple contour shows the position of the ground plane. More specifically, Fig. 8(a) shows the distribution of $|S_z|$ on XY plane (located at z = 1 mm) for $d = 1.5\lambda$, while Fig. 8(b) for $d = 2\lambda$. Array1 elements are fed with progressive phase shift of $-150°$, while Array2 elements are fed with progressive phase shift of $150°$. By using such progressive phase shifts, the main beam of each array is pointing towards the half of the space where the other array is located. The peak PD, when the two arrays operate simultaneously, decreases with increasing the distance d between them (see Fig. 8 right-hand side). In other words, by increasing d peak PD, when the two arrays operate simultaneously, approaches the peak PD, when only one array radiates at the time.

Table IV shows the results for the critical distance d at which the two antenna arrays are decoupled. The data are presented in terms of wavelengths. As one can see the critical distance is antenna dependent. The maximum physical

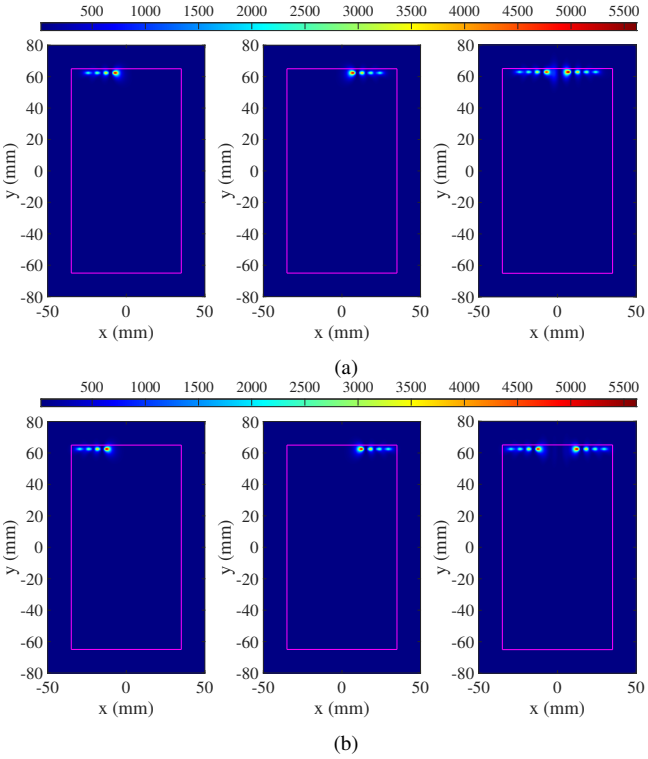

Fig. 8: Distribution of $|S_z|$ (in W/m^2) for Dipole2 in parallel case at 28 GHz (left-hand side - only Array1 transmits, center - only Array2 transmits, and right-hand side - both Array1 and Array2 transmit simultaneously; elements of Array1 are fed with progressive phase shift of $-150°$ while of Array2 of $150°$). The arrays are separated at: (a) $d = 1.5\lambda$, and (b) $d = 2\lambda$.

distance between the two arrays found needed for decoupling: 1) for parallel oriented arrays is around 32 mm (3λ at 28 GHz found for Dipole1); and 2) perpendicular oriented arrays is around 27 mm (similar between 2.5λ at 28 GHz found for Patch2 and 3.5λ at 39 GHz found for Patch1). It should be kept in mind that these results are approximate since the step used for finding the critical distance was of 0.5λ in order to limit the number of studies.

TABLE IV: Critical distance needed for decoupling of two antenna arrays in parallel and perpendicular case.

Antenna array	Critical distance d (λ) for parallel/perpendicular orientation		
	26 GHz	28 GHz	39 GHz
Patch1	1.5/1.5	1.5/1.5	3.5/3.5
Patch2	1/2	1/2.5	1/1.5
Dipole1	2.5/1.5	3/1.5	3/1.5
Dipole2	1.5/1.5	2/1.5	2/1.5

VII. Conclusion

This paper has presented two studies related to test reduction for handset mmWave antenna arrays. The findings in the paper are for patch and dipole antenna arrays as these antennas have been chosen since they are expected to be used for 5G mmWave mobile terminal. Each array has been made of 4-antennas, as this is the number of antennas currently considered to be deployed in an UE.

The first study has dealt with determining the size of the exposed volume around phased antenna arrays out of which the value of the PD is 13 dB below the global peak PD. The exposed volume defined through the components of the PD is larger than the volume found when the norm of the PD is considered. Criterion for considering the PD distribution symmetrical has been introduced. Following this definition, even when the array is not symmetrically placed with respect to the width/length of the edge of the ground plane, the results in more than a half of the cases are symmetrical. The latter means 50% less test time will be needed. The size of the volume in many cases is independent on the position of the array along the edge of the ground plane. Future work will deal with finding the boundary when averaging over a certain area is employed.

The second study has been focused on determining the critical distance between two 4-element arrays. This is the distance for which the peak PD emitted by any of the arrays (when only one operates at the time) is similar to the peak PD emitted when the two arrays operate simultaneously. If the distance between two arrays is known and by using the provided information, it can be judged whether the test when the two arrays transmitting simultaneously can be omitted. That is, the finding in this study can be used for reducing the number of PD measurements.

Acknowledgment

The authors would like to thank Kenneth H. Joyner at Mobile & Wireless Forum, Kai Niskala at Samsung Electronics Co. Ltd., Bo Xu and Davide Colombi at Ericsson AB, and Zhinong Ying at Sony Corporation for helpful discussion.

References

[1] W. Hong, K. Baek, Y. Lee, Y. Kim, and S. Ko, "Study and prototyping of practically large-scale mmwave antenna systems for 5G cellular devices," *IEEE Commun. Mag.*, vol. 52, no. 9, pp. 63–69, 2014.

[2] W. Roh, J. Seol, J. Park, B. Lee, J. Lee, Y. Kim, J. Cho, K. Cheun, and F. Aryanfar, "Millimeter-wave beamforming as an enabling technology for 5G cellular communications: theoretical feasibility and prototype results," *IEEE Commun. Mag.*, vol. 52, no. 2, pp. 106–113, 2014.

[3] "The 5G infrastructure public private partnership: the next generation of communication networks and services," [Online]. Available: https://5g-ppp.eu/wp-content/uploads/2015/02/5G-Vision-Brochure-v1.pdf, accessed: 2020-05-16.

[4] *User Equipment (UE) radio transmission and reception; Part 2: Range 2 Standalone*, TS 38.101-2, 3GPP, Rev. 16.0.0, June 2019.

[5] B. Xu, K. Zhao, Z. Ying, D. Sjöberg, W. He, and S. He, "Analysis of impacts of expected RF EMF exposure restrictions on peak EIRP of 5G user equipment at 28 GHz and 39 GHz bands," *IEEE Access*, vol. 7, pp. 20 996–21 005, 2019.

[6] *General aspects for User Equipment (UE) Radio Frequency (RF) for NR*, TR 38.817-01, 3GPP, Rev. 16.1.0, Sept. 2019.

[7] D. Colombi, B. Thors, and C. Törnevik, "Implications of emf exposure limits on output power levels for 5G devices above 6 GHz," *IEEE Antennas Wireless Propag. Lett.*, vol. 14, pp. 1247–1249, 2015.

[8] S. S. Zhekov and G. F. Pedersen, "Over-the-air evaluation of the antenna performance of popular mobile phones," *IEEE Access*, vol. 7, pp. 123 195–123 201, 2019.

[9] K. Zhao, Z. Ying, and S. He, "EMF exposure study concerning mmWave phased array in mobile devices for 5G communication," *IEEE Antennas Wireless Propag. Lett.*, vol. 15, pp. 1132–1135, 2016.

[10] B. Thors, D. Colombi, Z. Ying, T. Bolin, and C. Törnevik, "Exposure to RF EMF from array antennas in 5G mobile communication equipment," *IEEE Access*, vol. 4, pp. 7469–7478, 2016.

[11] ICNIRP, "Guidelines for limiting exposure to electromagnetic fields (100 kHz to 300 GHz)," *Health Phys.*, vol. 118, no. 5, pp. 483–524, May 2020.

[12] *Radiofrequency Radiation Exposure Limits*, FCC, Washington, DC, USA, 2013.

[13] *Notice of Proposed Rulemaking*, FCC, Washington, DC, USA, 2015.

[14] Technical Analysis Branch, Office of Engineering and Technology, FCC. (Oct. 2018). *RF exposure: Order/NPRM issues.*, [Online]. Available: https://transition.fcc.gov/oet/ea/presentations/files/oct18/5.1-TCB-RF-Exposure-OrderNPRM-Issues-MD.PDF, accessed: 2020-05-16.

[15] *IEEE Standard for Safety Levels with Respect to Human Exposure to Electric, Magnetic, and Electromagnetic Fields, 0 Hz to 300 GHz*, IEEE Standard C95.1-2019, 2019.

[16] Y. Hashimoto, A. Hirata, R. Morimoto, S. Aonuma, I. Laakso, K. Jokela, and K. R. Foster, "On the averaging area for incident power density for human exposure limits at frequencies over 6 GHz," *Phys. Med. Biol.*, vol. 62, no. 8, pp. 3124–3138, Mar. 2017.

[17] T. Nakae, D. Funahashi, J. Higashiyama, T. Onishi, and A. Hirata, "Skin temperature elevation for incident power densities from dipole arrays at 28 Ghz," *IEEE Access*, vol. 8, pp. 26 863–26 871, 2020.

[18] E. Carrasco, D. Colombi, K. R. Foster, M. Ziskin, and Q. Balzano, "Exposure assessment of portable wireless devices above 6 GHz," *Radiat. Prot. Dosim.*, vol. 183, no. 4, pp. 489–496, June 2019.

[19] T. Wu, T. S. Rappaport, and C. M. Collins, "Safe for generations to come: considerations of safety for millimeter waves in wireless communications," *IEEE Microw. Mag.*, vol. 16, no. 2, pp. 65–84, 2015.

[20] W. He, B. Xu, M. Gustafsson, Z. Ying, and S. He, "RF compliance study of temperature elevation in human head model around 28 GHz for 5G user equipment application: simulation analysis," *IEEE Access*, vol. 6, pp. 830–838, 2018.

[21] *Measurement Procedure for the Evaluation of Power Density Related to Human Exposure to Radio Frequency Fields From Wireless Communication Devices Operating Between 6 GHz and 100 GHz*, IEC TR 63170, Aug. 2018.

[22] B. Xu, K. Zhao, B. Thors, D. Colombi, O. Lundberg, Z. Ying, and S. He, "Power density measurements at 15 GHz for RF EMF compliance assessments of 5G user equipment," *IEEE Trans. Antennas Propag.*, vol. 65, no. 12, pp. 6584–6595, 2017.

[23] S. Pfeifer, E. Carrasco, P. Crespo-Valero, E. Neufeld, S. Kühn, T. Samaras, A. Christ, M. H. Capstick, and N. Kuster, "Total field reconstruction in the near field using pseudo-vector E-field measurements," *IEEE Trans. Electromagn. Compat.*, vol. 61, no. 2, pp. 476–486, 2019.

[24] J. Lundgren, J. Helander, M. Gustafsson, D. Sjöberg, B. Xu, and D. Colombi, "Near-field measurement and calibration technique for RF EMF exposure assessment of mm-wave 5G devices," Electromagnetic Theory Department of Electrical and Information Technology Lund University Sweden, Tech. Rep. 7267, 2019. [Online]. Available: https://lup.lub.lu.se/search/ws/files/68771039/TEAT_7267.pdf

[25] M. Nesterova, S. Nicol, and Y. Nesterova, "Evaluating power density for 5G applications," in *Proc. IEEE 5G World Forum (5GWF)*, 2018, pp. 347–350.

[26] K. Sasaki, K. Li, J. Chakarothai, T. Iyama, T. Onishi, and S. Watanabe, "Error analysis of a near-field reconstruction technique based on plane wave spectrum expansion for power density assessment above 6 GHz," *IEEE Access*, vol. 7, pp. 11 591–11 598, 2019.

[27] *Measurement procedure for the assessment of specific absorption rate of human exposure to radio frequency fields from hand-held and body-mounted wireless communication devices – Part 1528: Human models, instrumentation, and procedures (Frequency range of 4 MHz to 10 GHz)*, IEC/IEEE 62209-1528, 2020.